Climate Dynamics manuscript No.
(will be inserted by the editor)

Can climate models represent the precipitation associated with extratropical cyclones?

Matt Hawcroft · Len Shaffrey · Kevin Hodges · Helen Dacre

Received: date / Accepted: date

Matt K. Hawcroft

Department of Meteorology, University of Reading, Reading, UK

Tel.: +441183787037

E-mail: m.hawcroft@exeter.ac.uk

Present address: College of Engineering, Mathematics and Physical Sciences, University of Exeter, Exeter, UK

Len C. Shaffrey

National Centre for Atmospheric Science-Climate and Department of Meteorology, University of Reading, Reading, UK

Kevin I. Hodges

National Centre for Earth Observation, Environmental Systems Science Centre, University of Reading, Reading, UK

Helen F. Dacre

Department of Meteorology, University of Reading, Reading, UK

Abstract Extratropical cyclones produce the majority of precipitation in many regions of the extratropics. This study evaluates the ability of a climate model, HiGEM, to reproduce the precipitation associated with extratropical cyclones. The model is evaluated using the ERA-Interim reanalysis and GPCP dataset. The analysis employs a cyclone centred compositing technique, evaluates composites across a range of geographical areas and cyclone intensities and also investigates the ability of the model to reproduce the climatological distribution of cyclone associated precipitation across the Northern Hemisphere. Using this phenomena centred approach provides an ability to identify the processes which are responsible for climatological biases in the model. Composite precipitation intensities are found to be comparable when all cyclones across the Northern Hemisphere are included. When the cyclones are filtered by region or intensity, differences are found, in particular, HiGEM produces too much precipitation in its most intense cyclones relative to ERA-Interim and GPCP. Biases in the climatological distribution of cyclone associated precipitation are also found, with biases around the storm track regions associated with both the number of cyclones in HiGEM and also their average precipitation intensity. These results have implications for the reliability of future projections of extratropical precipitation from the model.

Keywords Precipitation · Extratropical cyclones · Climate models · HiGEM · Reanalysis · Remote sensing data

1 Introduction

Extratropical cyclones (hereinafter "ETCs") play a key role in transporting energy and momentum polewards in the general circulation (**?**Kaspi and Schneider

2013) and have a major influence on the weather in the mid and high-latitudes. Over two-thirds of the climatological precipitation in much of Europe and North America is associated with ETCs and this figure can be as high as 90% in the main stormtrack regions (Hawcroft et al 2012; Catto et al 2012). In addition, the majority of large scale extreme precipitation events in the extratropics are associated with the passage of ETCs (Pfahl and Wernli 2012; Catto and Pfahl 2013). ETCs can have high socio-economic impacts from the winds, rain and associated flooding they can bring (Ulbrich et al 2003; Pitt 2008; Sibley 2010; de Leeuw et al 2014). For example, in the summer of 2007, flooding associated with ETCs caused major disruption in the UK and insurance claims of over £3bn (Pitt 2008; Pearson et al 2014).

An ability to reproduce the current climate is a necessary condition of having confidence in climate model projections. Assessing whether a climate model adequately represents cyclone associated precipitation is important in terms of quantifying the impact of any prospective changes in both mean and extreme cyclone associated precipitation in the future. In this paper, the ability of a climate model, HiGEM, to represent the precipitation associated with ETCs is assessed.

The response of the storm tracks to climate change is driven by a number of influences (see, for example, Held 1993; Woollings 2010) with the overall response being modulated by the interplay of opposing controls, such as changes in hemispheric temperature gradients (Lim and Simmonds 2009; Butler et al 2010; Harvey et al 2014). In addition, any changes in the behaviour of ETCs themselves represents another such driver of the response of the storm tracks to climate change. An ability to represent the mean behaviour of ETCs is an important component of model evaluation in the extratropics. Models must also be able to reproduce the

magnitude and frequency of the most intensely precipitating ETCs and a realistic spectrum of event intensity - from weakly to intensely precipitating ETCs - to be considered reliable. This is particularly important since it is expected that the precipitation intensity of the most severe ETCs will increase in a warmer climate (Held 1993; Trenberth 1999) and that ETCs are often associated with high impact precipitation events in the extratropics (Pfahl and Wernli 2012; Catto and Pfahl 2013).

Studies of precipitation in climate models often use statistical analysis to evaluate model performance (e.g. Kendon et al 2012; Crétat et al 2014; Pearson et al 2014; Roy et al 2014) and climate models have previously been shown to have biases in both frequency and intensity of precipitation, even where the climatological accumulations compare closely to observations (Stephens et al 2010). In this paper, a process based approach is adopted by associating precipitation with a phenomenon - extratropical cyclones. This allows the analysis to move beyond a statistical evaluation of the precipitation climatology in the model to consider questions relating to the behaviour of these precipitation producing phenomena, for example, by linking precipitation biases to ETC frequency. This is particularly important given it is not clear that ETCs will respond to a change in climate in the same way as other precipitation producing phenomena, such as convective storms.

Cyclone tracking and compositing techniques are increasingly used in analyses of ETCs (e.g. Field and Wood 2007; Catto et al 2010; Rudeva and Gulev 2011). This study combines compositing with climatological analysis using techniques developed in Hawcroft et al (2012) and further applied in Zappa et al (2014) to provide a comprehensive evaluation of a climate model's ability to represent precipitation associated with ETCs.

The focus of this study is on winter (December-February, DJF) precipitation since this is the season where the majority of total annual precipitation falls in many regions of the Northern Hemisphere extratropics and when the main storm-tracks are at their most active. Anomalies in wintertime precipitation can also play a role in contributing to the onset of summertime droughts and heatwaves via deficits in soil moisture (e.g Ferranti and Viterbo 2006; Della-Marta et al 2007; Vautard et al 2007; Wang et al 2011) such that an inability to represent the winter precipitation climatology of the extratropics may have more far reaching effects in climate model projections.

The paper is structured as follows. In Section 2 the High-Resolution Global Environmental Model (HiGEM), ECMWF Interim Re-analysis (ERA-Interim) and Global Precipitation Climatology Project (GPCP) remote sensing dataset are introduced. The cyclone tracking algorithm is also discussed in addition to a summary of the technique applied to create and evaluate climatologies of ETC associated precipitation. Section 3 evaluates composite precipitation associated with ETCs in HiGEM. Section 4 considers the ability of HiGEM to reproduce the climatological distribution of ETC associated precipitation. A summary and conclusions are provided in Section 5.

2 Data and Methods

Many studies use renanalyses to evaluate the behaviour of climate models, with reanalysis being used as a proxy for the real world (in the ETC literature examples include Bengtsson et al 2006, 2009; Catto et al 2010; Hodges et al 2011). At the scale of ETCs, renanalyses may not be strongly constrained by observations

due to the location and nature of these phenomena, since many ETCs occur over oceans and many of the key processes which govern their behaviour (such as latent heat release) occur away from the surface. This introduces uncertainty in the renalysis product. Remotely sensed data may be employed to constrain the performance of reanalyses and may also be employed to directly evaluate climate models. This study therefore uses both reanalysis (ERA-Interim) and remote sensing data (GPCP) to evaluate the HiGEM climate model.

2.1 ERAI

The ERA-Interim (ERAI) reanalysis (Dee et al 2011; Simmons et al 2007) uses a 4D-Var data assimilation system to incorporate observations over a 12-hour analysis period, with forecasts commencing at 00:00UTC and 12:00UTC, and has a spectral resolution of T255 (approximately 80km/0.7° in the mid-latitudes). The ERAI model is based around the ECMWF's Integrated Forecast System (IFS) cycle Cy31r2, which was used for operational forecasting at ECMWF from 12 December 2006 until 5 June 2007. ERAI has 60 model levels, with an atmospheric top at 0.1 hPa. Precipitation is not an analysed field and in this paper is taken from short-range forecast accumulations, discussed in section 2.1.1. Data is available for the period of the GPCP data (see section 2.2) making ERAI particularly suitable for this study. The climatological precipitation and total precipitation associated with ETCs in the Northern Hemisphere have been shown to compare well to GPCP by Hawcroft et al (2012).

2.1.1 Spin-up in ERAI

Given the requirement to have daily accumulations centred on 12:00UTC for comparison to GPCP, it would be possible to use either (1) a continuous 24-hour accumulation from a single forecast for each day or (2) two 12 hour accumulations from successive forecasts. During the first several hours of forecasts, the precipitation field is affected by spin-up (see Kållberg 2011). As such, the forecast periods utilised in this study are accumulations from 12 to 24-hours from forecasts starting at 12:00UTC the previous day and 00:00UTC on the day of interest. The two forecast accumulations are combined to provide daily precipitation estimates. The 12 to 24-hour forecast estimates have previously been found to compare well to gridded rain gauge observations (Simmons et al 2010) and recent work indicates that the lead time used in this paper offers the best estimates available from ERAI given the daily accumulations required for this study (Hawcroft et al 2012; de Leeuw et al 2014). A further evaluation, investigating any spin-up/adjustment (as the model is initialised) or model drift (as the forecast increases in length and the model is no longer closely constrained by observations) was performed for this study, confirming the propriety of the 12-24 hour lead times. This is further discussed in the Appendix to this paper.

The ERAI data used in this study is from DJF 1998/99-2007/08, providing a decade of data which overlaps with the availability of GPCP. Analysis on a longer period of data (from 1979 onwards) to assess uncertainty which may arise from decadal variability did not materially affect the conclusions.

2.2 GPCP

The Global Precipitation Climatology Project one-degree-daily (GPCP) precipitation dataset (Huffman et al 2001, 2009; Adler et al 2003) is a 1°x1° gridded dataset that combines multiple satellite estimates and rain gauge data to produce daily accumulations centred on 12:00UTC. The satellite estimates are tuned using monthly gauge observations. The GPCP data is available from December 1996 to the present. The period DJF 1998/99-2007/08 is used here, which is the same as the ERAI data.

GPCP has been evaluated against rain gauge observations, generally performing well (e.g. Nicholson et al 2003), though it has been shown that GPCP underestimates very high intensity events in the United States (McPhee and Margulis 2005) and India (Joshi et al 2013) and overestimates them at high-latitudes (Bolvin et al 2009). It is not possible to systematically verify satellite derived estimates over the oceans and other regions where gauge sampling is sparse (John et al 2009) which increases uncertainty in the precipitation estimates over oceans.

There remains uncertainty in the precipitation estimates derived from both satellite observations (Kummerow et al 2006; Field and Wood 2007; Stephens et al 2010) and from reanalysis (Hou et al 2001). However, neither the GPCP or ERAI datasets provide estimates of uncertainty for precipitation. As such, the use of multiple datasets to evaluate HiGEM allows greater ability to assess uncertainty with respect to the remotely sensed data and the reanalysis.

2.3 HiGEM

The model evaluated in this study is HiGEM1.2 (Shaffrey et al 2009), which is based on the U.K. Met Office Hadley Centre Global Environmental Model (HadGEM1). HiGEM is a higher resolution version of HadGEM1, in both atmosphere and ocean. The horizontal resolution is $0.83^\circ \times 1.25^\circ$ (N144) for the atmosphere, and $^1/_3^\circ \times ^1/_3^\circ$ globally for the ocean and sea ice. The atmosphere has 38 vertical levels with a model top at 39km. The atmospheric dynamics of HiGEM use non-hydrostatic, fully compressible, deep-atmosphere equations and a semi-Lagrangian advection scheme for all prognostic variables except density (Davies et al 2005). Detailed description of the model formulation can be found in Shaffrey et al (2009); Johns et al (2006); Martin et al (2006); McLaren et al (2006) and references therein. Precipitation is a diagnostic quantity in both the large-scale precipitation and convection schemes with precipitation estimates produced at the surface at each timestep. HiGEM has previously been shown to be capable of capturing the synoptic scale circulation features of composite ETCs when compared to reanalysis (Catto et al 2010).

In this study, the precipitation from HiGEM is accumulated during a 24-hour period centred on 12:00UTC in order to provide data comparable to GPCP (see section 2.2). Data is available for 80 consecutive years in a control run forced with late 20^{th}-century radiative forcings. Data from the first 20 years of the integration is thought to be affected by spin-up effects since this is the period it takes for the net top of the atmosphere (TOA) radiation flux to stabilise (Shaffrey et al 2009). Analysis of decadal variability within the 80 year period indicates that the precipitation associated with ETCs exhibits low variability - including during the

first 20 years (see Appendix). A decade of winter (DJF) seasons starting 30 years into the model run is used in this study to provide a period of sufficient sampling for which there is also a period of comparable length in the observations/renalysis data for comparison.

2.4 Tracking and compositing methodology

The feature tracking algorithm used in this study (e.g. Hodges 1994, 1995, 1999, and further described in Hoskins and Hodges 2002 and Bengtsson et al 2009), has previously been applied in studies of ETCs (e.g. Hoskins and Hodges 2002; Bengtsson et al 2006, 2007, 2009; Catto et al 2010; Hawcroft et al 2012). Northern Hemisphere ETCs are identified as features exceeding $1\times10^{-5}s^{-1}$ in the 850 hPa relative vorticity field, truncated to T42. Features identified poleward of 30N, with a lifetime of at least 2 days and which travel at least 1000 km are retained as ETCs and included in the analysis. The sensitivity of the results to these thresholds has been assessed through investigating the impact of a relaxation of either the time or distance criteria. Conclusions were insensitive to changing these thresholds.

Tracks are identified in 6-hourly fields in HiGEM and ERAI and are then degraded to daily resolution with points at 12:00 UTC retained. Tracks of the ETCs used for GPCP are identified in the analysed ERAI data, which represents a best guess of the state of the atmosphere, and the precipitation fields are centred on the analysed location at 12UTC. For ERAI, the ETCs are identified in the 12-hour lead time forecast vorticity making their locations consistent with the forecast precipitation accumulations. In HiGEM, the model is run in climate mode, so

precipitation and vorticity are simply extracted from the model fields and are self-consistent.

The compositing methodology employed here has previously been applied in studies of ETCs (e.g. Bengtsson et al 2007, 2009; Catto et al 2010; Dacre et al 2012; Dacre and Gray 2013). It involves several steps and is discussed in detail in Catto et al (2010). To summarise the procedure, first the tracks to be composited are identified and selected. The precipitation field is then extracted on a radial grid centred on each of the identified cyclone points. A time within each track's lifecycle is chosen for compositing, which in this study is the time of maximum precipitation intensity based on the average precipitation within 5° of the ETC centre. The precipitation, for each ETC at the relevant timestep, is then averaged across all ETCs to create a composite. The ETCs are not rotated to their direction of travel prior to compositing. This was not possible due to the technique employed to extract ETCs within specified regions. The results for composites across the whole Northern Hemisphere were not sensitive to using rotation. Sensitivity of the results to the choice of a 5° radial cap for the identification and selection of ETCs to be included in these composites was tested by increasing the size of this cap to 10° and 15°, which would capture precipitation more distant from the storm centre, such as that on an extended trailing cold front. The conclusions were insensitive to changing the cap size. An analysis of the tracks identified using each radial cap (not shown) shows that the tracks selected are largely identical irrespective of the radius used. When producing composites, points with zero precipitation are included in this study. The mean precipitation and intensity distributions would differ if zero values were not included (see Rossow et al 2013). In this study, where

confidence intervals are expressed with respect to mean composite precipitation rates, they have been calculated using bootstrapping.

It has previously been shown that the maxima of precipitation in ETCs typically occurs prior to the maximum dynamical intensity as the latent heat release associated with the precipitation acts to intensify the storm (Bengtsson et al 2009; Dacre et al 2014). Given the focus of this study is on precipitation, cyclones are subset based on their precipitation intensity, rather than a dynamical field (e.g. vorticity).

2.5 Precipitation climatologies methodology

The analysis of precipitation climatologies performed in section 3.2 is that developed in Hawcroft et al (2012) and further applied in Zappa et al (2014). Cyclones are identified using the tracking technique described in section 2.4 at 12UTC on each day. Precipitation within a 12° radial cap of an ETC centre is designated as being associated with an ETC. The choice of this radius is justified in Hawcroft et al (2012). The daily accumulated precipitation fields used in this part of the study are created in the same way as for the composite analysis. At each grid point, the precipitation produced within 12° of ETCs from all daily timesteps is accumulated to provide a climatology of storm associated precipitation. This is then compared to the total precipitation and the fraction of the total precipitation associated with ETCs is further evaluated.

To assess the contribution of the most extreme storms to the climatology, ETCs are subset by their maximum precipitation intensity (based on 5° areal average precipitation around the ETC centre). Sensitivity of the climatologies to subsetting

the storms using a larger cap to assess intensity was tested and did not influence the conclusions. Using these filtered extreme storms, the same methodology is applied to create climatologies of precipitation solely associated with the most heavily precipitating ETCs. Using this technique, the ability of the model to produce a realistic spectrum of storms, from weakly to heavily precipitating, is evaluated.

A further decomposition of ETC associated precipitation is also undertaken, using the same methodology as Zappa et al (2014) which is similar to that employed by Finnis et al (2007). Biases in the total storm associated precipitation climatology may be associated with errors in (1) the average ETC precipitation intensity, (2) the number of ETCs, or (3) a combination of the two. It is possible to separate these effects through considering the total Storm Associated Precipitation (SAP) at a gridpoint $P_{SAP}(x, y)$ to be a function of the total number of days when a gridpoint is within the radius of an ETC, $N(x, y)$, and the mean precipitation which falls at that gridpoint across these timesteps, $\mu(x, y)$, such that

$$P_{SAP} = N \cdot \mu, \tag{1}$$

N and μ can be calcuated for HiGEM (N_H, μ_H), GPCP and ERAI (N_E, μ_E). The results for GPCP and ERAI are comparable, so for simplicity only ERAI is shown here. Using this approach, it is possible to decompose the extent to which biases ($\triangle P_{SAP}$) in HiGEM are attributable to errors in N or μ as follows

$$\triangle P_{SAP} = N_H \cdot \mu_H - N_E \cdot \mu_E = (N_H - N_E) \cdot \mu_E + (\mu_H - \mu_E) \cdot N_e + (N_H - N_E) \cdot (\mu_H - \mu_E) \tag{2}$$

such that any biases in ETC associated precipitation can be attributed to errors in number, intensity or a cross—term associated with errors in both number and intensity.

3 Cyclone associated precipitation

3.1 Composite precipitation

In Figure 1 the track density for the datasets is shown for the 10 seasons analysed in this study. The broad patterns of ETC activity in HiGEM are comparable to ERAI (see also Catto et al 2011). The performance of HiGEM in this respect compares favourably relative to the CMIP5 models (see Zappa et al 2013). Examining Figure 1 in further detail, it can be seen that in HiGEM there is a higher track density in the central/western Pacific and lower density in the eastern Pacific when compared to ERAI. Differences in the spatial distribution of ETCs are also observed in the Atlantic.

3.1.1 Northern Hemisphere composite precipitation

In Figure 2 composites of precipitation from all ETCs (3662 in HiGEM and 3764 in ERAI/GPCP) are shown. In the innermost 5° of the composites, the precipitation averages vary from 6.98 to 7.67 mm day^{-1}. Maximum intensities (the highest single grid point in each composite) are 10.38/10.52/10.63 mm day^{-1} in HiGEM/ERAI/GPCP, respectively, and are not statistically distinguishable (at 95% confidence levels). In Table 1, which shows the average precipitation associated with composites of ETCs from the three datasets, ETCs are subset by intensity. HiGEM produces relatively more intensely precipitating ETCs though the mean precipitation values are generally not statistically different from one of the two observational datasets. For example, for the 200 most intensely precipitating storms the 5° radially averaged precipitation is 25.33/24.31/24.66 mm

303 day^{-1} in HiGEM/ERAI/GPCP, respectively, with 95% confidence intervals of
304 $\pm 0.55/0.57/0.75$ mm day^{-1}.

305 *3.1.2 Regional composite precipitation*

306 Given the majority of the ETCs which are incorporated into Figure 2 are over
307 the ocean, it is instructive to construct composites from each dataset using storms
308 from both continental and oceanic regions.

309 In Figure 3 composites of precipitation in the most intensely precipitating 200
310 ETCs from four regions are shown. The location of the Pacific, Atlantic, European
311 and North American regions sampled in these composites are shown in Figure
312 1. The selection of 200 ETCs is justified on the basis that it provides sufficient
313 sampling to reduce noise but also samples fully developed ETCs in all regions - in
314 the continental regions, sampling a large number of ETCs requires the inclusion
315 of weakly precipitating systems which may not exhibit the typical structure and
316 behaviour of ETCs. Precipitation intensities in these composites for 5° radii are
317 provided in Table 2.

318 In Figure 3, in the Atlantic, the maximum precipitation intensity in HiGEM
319 exceeds 30mm day^{-1} compared to maxima of 26mm day^{-1} in GPCP and ERAI.
320 The radial precipitation averages (Table 2) also reflect these intensity differences,
321 with 5° precipitation averages in HiGEM over 1mm day^{-1} greater than in GPCP
322 and ERAI (though this difference is only significant at a 95% level with respect to
323 ERAI). In the Pacific composites, the precipitation maxima exceed 32/30/27mm
324 day^{-1} in ERAI/HiGEM/GPCP. The radial precipitation averages (Table 2) in the
325 Pacific are, however, closely comparable across the datasets.

For the Europe region, the magnitude of the individual (single pixel) precipitation maxima are in better agreement than the oceanic composites across the three datasets, with peak composite precipitation, all falling within a range of 12.5-15.0 mm day^{-1}. The spatial extent of the region of peak precipitation is more extensive in GPCP leading to higher area averaged precipitation within the central 5° of the composites (Table 2). In the North America region, the maximum precipitation intensities in ERAI and GPCP are ∼25mm day^{-1} with a more intense maximum of 31mm day^{-1} in HiGEM.

The differences in precipitation rates across the regions can be better characterised through an analysis of the 200 individual storms which contribute to each composite. The storms are individually extracted and the precipitation around each storm is gridded into a 14400 point array (360°x20° with 1x0.5° resolution). Statistics are then derived from these 200 storms. In Figure 4 histograms of precipitation rates over all points in the 200 storms are shown. In these histograms, the 95% confidence interval in each bin is less than 0.21% in all cases, such that almost all bins are statistically separable across the datasets. Over 15% of points are non-precipitating in GPCP in both the Atlantic and Pacific ETCs, with fewer than 5% assigned as non-precipitating in both HiGEM and ERAI.

Analysing the points within 5° of each storm centre (not shown), where much of the heaviest precipitation associated with the WCB occurs, the proportion of gridpoints in GPCP with precipitation rates below 8mm day^{-1} is much greater than in ERAI and HiGEM (over 44% compared to less than 18% in both the Atlantic and Pacific) with correspondingly fewer gridpoints with higher precipitation rates. The differences between GPCP and ERAI/HiGEM in the Atlantic and Pa-

cific therefore appear to be associated with both the intensity of the most heavily precipitating gridpoints and also the frequency of non-precipitating gridpoints.

For the Europe region, Figure 4 shows that in GPCP over twice as many gridpoints have precipitation rates greater than 16mm day^{-1} compared to ERAI and HiGEM. The number of gridpoints that are non-precipitating is much higher in GPCP (over 22% compared to less than 8% in ERAI and HiGEM). The net result of these competing effects is that composite precipitation in Europe is higher in GPCP than in ERAI and HiGEM (see Figure 3 and Table 2). In the North America region, the composite precipitation intensities in ERAI and GPCP in Figure 3 and Table 2 are similar with more intense composite precipitation found in HiGEM. In Figure 4 it can be seen that HiGEM produces a greater number of gridpoints above 32mm day^{-1} than both ERAI and GPCP. As in other regions, the number of non-precipitating gridpoints in GPCP is significantly greater than in ERAI and HiGEM (over 23% compared to less than 12% and 8%, respectively).

In summary, though HiGEM generally compares well to both GPCP and ERAI when mean composite precipitation rates are evaluated across all Northern Hemisphere ETCs, differences occur as more intensely precipitating storms are analysed. The statistical distribution of precipitation intensities within the ETCs show that the mean precipitation rates may mask differences in intensity distribution.

3.2 Cyclone associated precipitation climatology

It has previously been shown in Hawcroft et al (2012) that estimates of the total precipitation in the Northern Hemisphere produced by ETCs ('storm associated precipitation') in ERAI and GPGP agree well. In Figure 5 the total precipita-

tion, total storm associated precipitation and percentage of the total precipitation contributed by ETCs is shown for HiGEM, ERAI and GPCP.

Figure 5(a-c) shows that HiGEM is able to reproduce the broad precipitation structure of the two major stormtracks. There are, however, biases in the location of the maxima in both stormtracks (i.e. located too close to the western boundaries of the Pacific and Atlantic) and an over-extension of the Atlantic stormtrack towards Iceland. The total precipitation within both the Atlantic and Pacific storm tracks reaches 7mm day^{-1} in DJF in GPCP/ERAI. In HiGEM, this peaks at 10mm day^{-1} in the Pacific and 9mm day^{-1} in the Atlantic. The high precipitation bias in the total precipitation in the storm track regions is also present in the storm associated precipitation climatology in HiGEM (Figure 5(d-f)). In the Pacific, the maximum storm associated precipitation reaches 8mm day^{-1} in HiGEM compared to 5-6mm day^{-1} in GPCP/ERAI. In the Atlantic, the maximum storm associated precipitation is in excess of 7mm day^{-1} in HiGEM and can again be contrasted with the 5-6mm day^{-1} maxima in GPCP/ERAI.

Figure 5(g-i) show the percentage of the total precipitation climatology which is contributed by ETCs, with ETCs contributing over 50% of total precipitation in much of the Northern Hemisphere. In some locations this contribution can exceed 90%. The percentage of total precipitation produced by HiGEM can generally be considered within the bounds of observational uncertainty in many regions given the differences observed between ERAI and GPCP. However, around the Atlantic and Pacific stormtracks the spatial extent of the region where over 80% of total precipitation is contributed by ETCs is overestimated in HiGEM. Where the percentage figures in HiGEM agree with ERAI and GPCP, but the total precipitation/storm associated precipitation is overestimated (such as in the storm tracks),

this implies that there may be some deficiencies in the representation of precipitation in HiGEM - in the storm tracks, too much precipitation is being produced by ETCs but too much precipitation is also produced when ETCs are not present.

3.2.1 Decomposition of bias

The number of ETCs in the Pacific/Atlantic stormtracks in HiGEM exhibits spatial differences when compared to ERAI (see Figure 1). There are also differences in the composite precipitation estimates across the regions (as shown in Figure 3). The impact on the climatology of these differences in number and intensity can be more fully decomposed to assess the contribution of errors in (1) storm number and (2) average storm precipitation intensity to the total storm associated precipitation bias in HiGEM using the technique introduced in Section 2.5.

This analysis is shown in Figure 6 and the cross—term is generally small (Figure 6(e)). The regions with large bias in storm associated precipitation in HiGEM (notably in the Pacific and Atlantic stormtracks and in the eastern Mediterranean) are primarily associated with errors in the average intensity of ETCs (Figure 6(d)). The positive precipitation bias in the central and western Pacific and north east Atlantic is further enhanced by excessive ETC number (Figure 6(c)). In other regions, such as the western Atlantic, an underestimate of storm number acts to modulate and in some instances reverse high biases in average precipitation intensity. In the central Atlantic, the significant underestimate in average intensity is the dominant term. The spatial structure of these biases can, in part, be related to SST errors in HiGEM (see Shaffrey et al 2009, Figure 3), such as a local cold bias in SSTs situated in the central Atlantic which is spatially coincident with an underestimate in precipitation. Keeley et al (2012) found this local precipitation

underestimate disappeared when the model was forced with observed SSTs. Across the extratropics, the net effect of these two factors (number and intensity) is to leave a complex pattern of over/underestimation of storm associated precipitation in HiGEM.

3.2.2 The contribution of heavily precipitating cyclones to the total storm associated precipitation

The differences in the storm associated precipitation climatology between HiGEM and GPCP/ERAI are related to both the spatial distribution of ETCs and differences associated with the average amount of precipitation produced by ETCs. If the distribution of storm associated precipitation from heavily and lightly precipitating events differs (e.g. too much precipitation coming from a small number of heavy events rather than a greater number of light events) this has implications for the temporal distribution of precipitation at any given location, which is important for flooding, droughts and agriculture and also the plausibility of future projections of any change in such events that might be derived from integrations of HiGEM.

Figure 7 shows the contribution of ETCs to the total storm associated precipitation climatology throughout their lifecycle as a function of each ETC's maximum precipitation intensity. In HiGEM, the relative contribution of the most intense storms is greater than in ERAI/GPCP. For example, in HiGEM, the most intense 10% of ETCs produce over 30% of the total storm associated precipitation compared to less than 25% in both ERAI and GPCP. As a result, substantially less precipitation is produced by weaker ETCs in HiGEM. Greater differences are seen between ERAI and GPCP for weaker intensities, though the contribution of

weaker ETCs in HiGEM lies significantly outside the bounds of uncertainty between ERAI and GPCP. For the weakest 60% of ETCs, HiGEM/ERAI/GPCP produce contributions of 21.1/30.8/26.2%, respectively. These biases again imply that precipitation processes have some deficiencies in HiGEM.

4 Summary and conclusions

This study has investigated whether HiGEM is able to reproduce the precipitation associated with ETCs using a tracking and compositing analysis. ETCs are composited at the time of their most intense precipitation and the contribution of ETCs across their whole lifecycle to total precipitation in the Northern Hemisphere has been assessed. The output of the model has been evaluated against ERAI reanalysis and GPCP remote sensing precipitation estimates. Given the importance of precipitation associated with ETCs to the total precipitation climatology and uncertainties about how ETCs will respond in a changing climate, evaluating the ability of climate models to reproduce precipitation associated with ETCs assists in establishing the likelihood that their projections of future precipitation change are reliable.

This study has taken a process based approach to the evaluation of HiGEM by identifying ETCs and evaluating processes around them. Such an approach provides a platform to link biases in physical processes in the climate system with the representation of a specific, identified phenomena and provides a different perspective to a simply statistical evaluation of the model.

The key findings of this study as are follows

- Composites of precipitation associated with all Northern Hemisphere ETCs in HiGEM compare well to ERAI and GPCP. See Figure 2.
- Differences in composite precipitation between HiGEM and ERAI/GPCP are found when ETCs are selected by region. Differences in these composites are also found between ERAI and GPCP. Within the composites, the statistical distribution of precipitation rates is found to vary across the datasets. HiGEM produces a greater frequency of very intense (over 64mm day^{-1}) precipitation than both GPCP and ERAI. See Figures 3 and 4.
- HiGEM is able to reproduce the broad patterns of precipitation associated with the Northern Hemisphere storm tracks. Localised biases are associated with both the numbers of ETCs and the average precipitation intensity of ETCs, though the patterns of these biases are spatially complex and of varying sign. In the Pacific, HiGEM produces too many ETCs which typically produce too much precipitation. In the Atlantic, a more complex pattern is observed, with weaker precipitation intensity related to local cold SST biases. See Figure 6.
- HiGEM is found to produce a disproportionately high fraction of storm associated precipitation from the most intensely precipitating ETCs, with over 30% of total storm associated precipitation coming from the most intense 10% of ETCs compared to less than 25% in ERAI/GPCP, with a resultant underestimate of the fraction of precipitation produced by weaker ETCs. See Figure 7.

Over the ocean, the mean distribution of precipitation around composites of intensely precipitating ETCs in GPCP and ERAI masks differences in the statistical distribution of precipitation rates. This introduces uncertainty into the observa-

tional estimates which are being used to evaluate HiGEM. These results indicate caution is required when validating model estimates of precipitation, particularly intense precipitation, over the extratropical oceans.

Hawcroft et al (2012) have previously shown that the storm associated precipitation climatologies in GPCP and ERAI are comparable. In this study HiGEM is shown to over estimate both the total precipitation and storm associated precipitation (by up to 3mm day^{-1}) around the main stormtrack regions in the Atlantic and Pacific. It has also been shown that intense ETCs produce too much of the total storm associated precipitation in HiGEM when compared to ERAI and GPCP. Similar biases have been found when intense precipitation associated with fronts has been evaluated in the ACCESS model, which is based on a similar model to HiGEM (Catto et al 2013).

Given the importance of ETCs to the total precipitation climatology (Hawcroft et al 2012) and the fact many large scale extreme precipitation events are associated with ETCs (Pfahl and Wernli 2012; Catto and Pfahl 2013), these results are important. The identified biases may have implications for the reliability of any projections of the behaviour of ETCs, extreme extratropical precipitation events or the frequency of precipitation derived from HiGEM using idealised future scenarios. The techniques used in this study have been applied to evaluate the CMIP5 dataset in the Mediterranean (Zappa et al 2014) and could be extended to the whole Northern Hemisphere to understand whether the precipitation intensity errors observed here are typical of GCMs.

The precipitation biases observed in HiGEM may be related to the large scale dynamics of the model (including SST biases) and may also be influenced by a poor representation of processes in ETCs, such as the location and magnitude of latent

heat release. Catto et al (2010) have shown that the large-scale features of ETCs are well represented in HiGEM when compared to the ERA-40 reanalysis (Uppala et al 2005) though the structure of the warm conveyor belt, where much precipitation is produced and significant latent heat is released, is much deeper in HiGEM (using relative humidity as a proxy for cloud) than ERA-40. Any biases in the processes which produce precipitation around ETCs may have upscale dynamical effects. The amount of precipitation produced by an individual cyclone is closely related to the column integrated latent heat release since condensational heating associated with precipitation is one of the primary diabatic processes which occurs in ETCs (Joos and Wernli 2011). For example, Willison et al (2013) found reducing latent heating in ETCs reduced the intensity of the Atlantic stormtrack in a series of idealised experiments. The representation of latent heating around ETCs and its relationship with the evolution and behaviour of ETCs in HiGEM is the subject of ongoing investigation.

Acknowledgements MKH is supported by the Natural Environment Research Council's project 'Testing and Evaluating Model Predictions of European Storms' (TEMPEST). The authors would like to thank three anonymous reviewers for their insightful and helpful comments in improving this manuscript.

Appendix

Decadal variability in HiGEM

The data used in this study is taken from a single decade of an 80 year integration of the model forced with late 20^{th}-century radiative forcings. Figure 8 shows the percentage of the total precipitation contributed by ETCs in each of these decades. It can be seen that though there are small variations in the locations of the highest precipitation accumulations, associated

with variability in the storm track locations, the biases in the model climatology relative to the observations remain consistent across the decades.

Spin-up in ERAI

The ERAI reanalysis (Dee et al 2011; Simmons et al 2007) uses a 4D-Var data assimilation system to incorporate observations over a 12-hour analysis period, with forecasts commencing at 00:00UTC and 12:00UTC. Precipitation is not an analysed field and must therefore be taken from short-range forecast accumulations. During the first several hours of the forecast simulation, the precipitation field (and many other fluxes and tendencies) is affected by "spin-up" as the model adjusts from the initialised fields, such that the estimates at the start of the forecast period are less robust than at later lead times (see Kållberg 2011). Moving too far from the start of the forecast also leads to degradation of the precipitation estimates. Given these issues, a suitable window must be chosen for the accumulations to be used in this study. The primary constraints on the selection of an appropriate period is the desire to use the GPCP dataset in this work. The GPCP dataset provides daily total precipitation estimates from 00-24UTC. Further, the ERAI forecasts are initialised every 12 hours so any accumulations must be selected from continuous 12 or 24 hour periods in the forecast.

Given the requirement to have daily accumulations centred on 12:00UTC, it would be possible to use either (1) a continuous 24-hour accumulation from a single forecast for each day or (2) two 12 hour accumulations from successive forecasts. To assess this, evaluating any spin-up/adjustment (as the model is initialised) or model drift (as the forecast increases in length and the model is no longer closely constrained by observations) is required. The adjustment/drift effect can be more readily demonstrated using shorter accumulation periods. In this analysis, given the 12 hour or greater accumulation periods required for comparison to GPCP, 0-12, 12-24 or 24-36 hours are likely candidate lead times for analysis. Longer forecasts are likely to degrade the quality of the estimates as the forecast model relaxes into a state which is less constrained by observations.

In Figure 9 composite precipitation taken from the 200 Atlantic storms in Figure 3 is shown. The results for other regions are not materially different. The composites show accu-

mulated precipitation at variable lead times from 0-3, 12-15, 24-27 and 36-39 hours where the accumulation is from each 3 hour window.

The storm position is centred on the analysed location at the time the precipitation fields are extracted, since to sample the forecast location would be laborious and add little value to the analysis. As such, there is some spatial offset in the location of the maxima in the longer lead times. This is because ETCs tend to propagate too slowly in the forecast model, giving the impression that the precipitation maxima move closer to the storm centre as lead time increases (see Froude et al 2007a,b). It is clear that the 0-3 hour accumulation has lower accumulated precipitation than the longer lead times. It is also apparent that the intensity of the precipitation maxima steadily degrades with lead times beyond 12 hours.

This is further evident in the precipitation cross sections shown in Figure 10. Given the location of the precipitation maximum changes due to the storm centring, the cross-sections are shown for a number of locations, though the differences between the lead times remain clear. As a result of the adjustment effect in the 0-3 hour period and the steady decay observed in the precipitation maxima and structure in the 24 and 36 hour lead times, the forecast periods utilised in this study for comparison to GPCP are accumulations from 12 to 24 hours from forecasts starting at 12:00UTC the previous day and 00:00UTC on the day of interest, as shown in Figure 11. The two forecast accumulations are combined to provide daily precipitation estimates for comparison to GPCP. The 12 to 24-hour forecast estimates have previously been found to compare well to gridded gauge data (Simmons et al 2010), with longer lead times degrading the quality of the estimates (Kobold and Sušelj 2005). The results of de Leeuw et al (2014) also indicate that this lead time offers the best estimates available from ERAI given the daily accumulations required in this study.

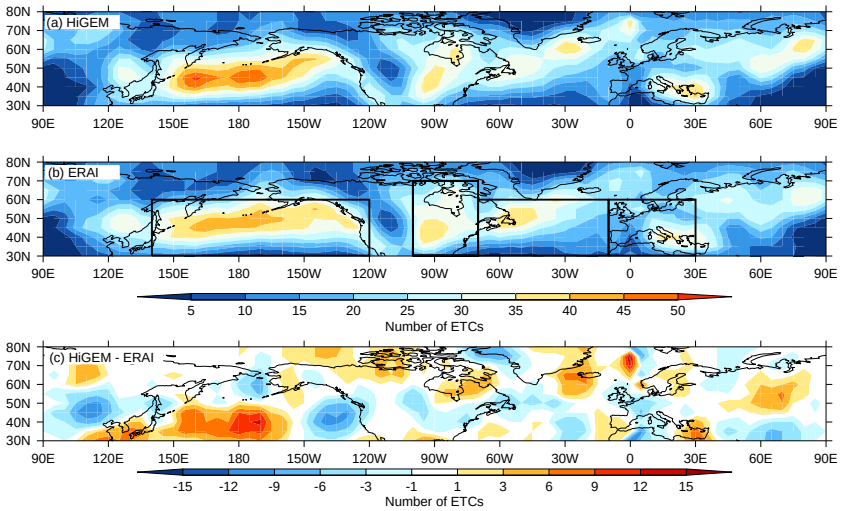

Fig. 1 Histogram of ETC track density in (a) HiGEM, (b) ERAI and (c) the difference between (a) and (b). Tracks from ERAI are used to identify ETCs in GPCP. The total number of ETCs per 5° across the 10 seasons used in this study is shown and the plots are smoothed over 3° to reduce noise. In the ERAI histogram, the Pacific, North American, Atlantic and European regions are shown which are used to subset the ETCs included in the composites in Figure 3 and statistics in Table 2.

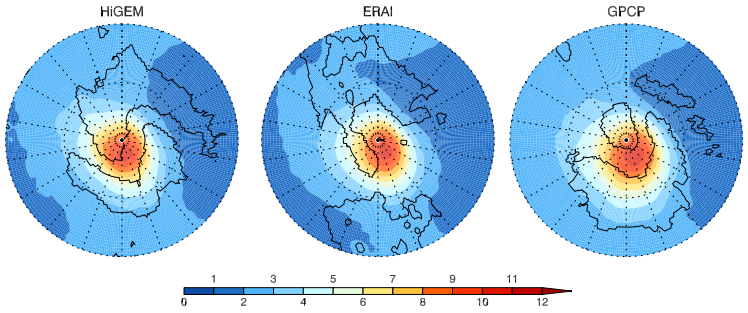

Fig. 2 Composite precipitation (mm day^{-1}) from all Northern Hemisphere ETCs in the HiGEM, ERAI and GPCP datasets for the 10 seasons used in this study. Composites have a 20° radius. The areas enclosed by black contours show where differences between the datasets are statistically significant at ≥95%. In the HiGEM composite, the 95% contour is shown with respect to GPCP. In the ERAI composite, the 95% contour is shown with respect to HiGEM. In the GPCP composite, the 95% contour is shown with respect to ERAI.

Northern Hemisphere ETCs					
	All	top 1000	top 500	top 200	top 100
HiGEM	7.67 (±0.22)	16.75 (±0.31)	20.60 (±0.41)	25.33 (±0.55)	28.33 (±0.65)
ERAI	7.54 (±0.21)	16.43 (±0.30)	20.05 (±0.39)	24.31 (±0.57)	26.91 (±0.88)
GPCP	6.98 (±0.21)	15.93 (±0.33)	19.90 (±0.47)	24.66 (±0.75)	28.25 (±1.08)

Table 1 Radially weighted precipitation averages for the 5° closest to the composite centres for all storms in the Northern Hemisphere (poleward of 30N) with storms further sub-sampled by their maximum precipitation intensity showing, for example, the average precipitation in the 100 most intense storms (mm day^{-1}). Sampling of storms is based on the average precipitation in a 5° radius from the ETC centre at the time of maximum precipitation. Confidence intervals (at 95%) are shown in brackets.

Regional ETCs					
	All	Atlantic	Pacific	Europe	North America
HiGEM	25.33 (±0.55)	19.02 (±0.67)	21.46 (±0.75)	9.03 (±0.29)	16.26 (±0.73)
ERAI	24.31 (±0.57)	17.51 (±0.49)	21.68 (±0.73)	9.13 (±0.29)	14.92 (±0.68)
GPCP	24.66 (±0.75)	17.93 (±0.67)	21.23 (±0.90)	13.12 (±0.49)	16.69 (±0.92)

Table 2 Radially weighted precipitation averages for the 5° closest to the composite centres for the 200 most intensely precipitating ETCs in all of the Northern Hemisphere (poleward of 30N) and in each region (mm day^{-1}). Sampling of storms is based on the average precipitation in a 5° radius from the ETC centre at the time of maximum precipitation within each region. Confidence intervals (at 95%) are shown in brackets. The regions are shown in Figure 1.

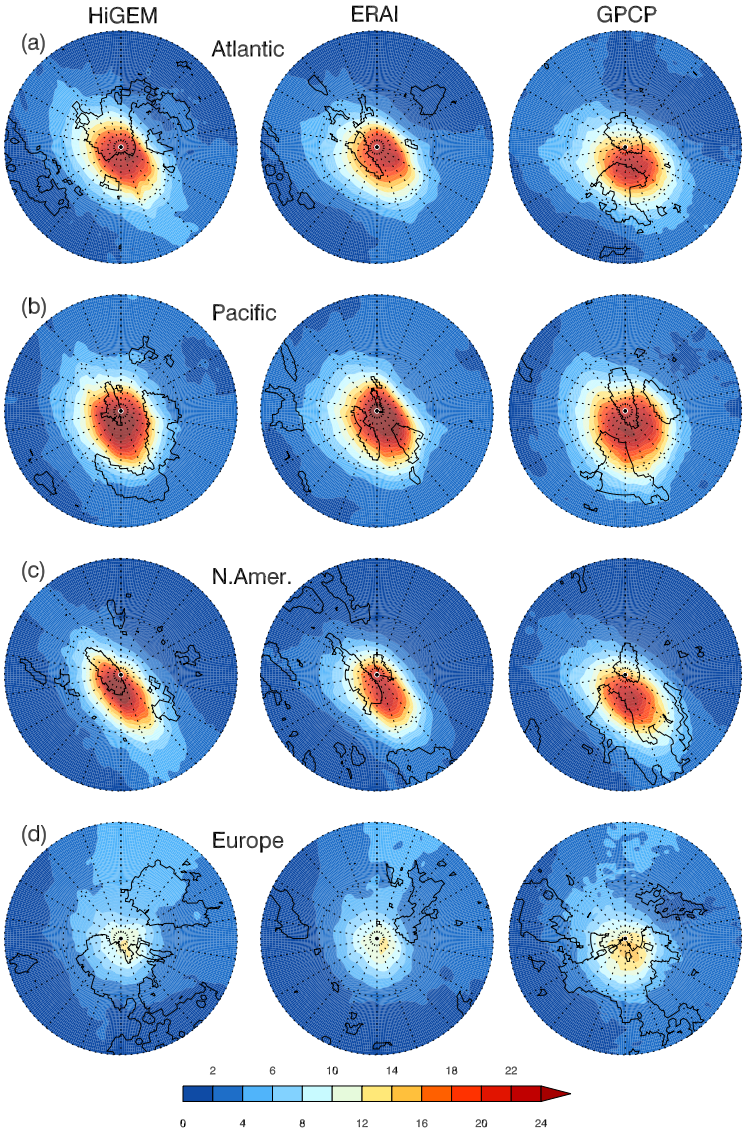

Fig. 3 Composite precipitation in HiGEM, ERAI and GPCP for the (a) Atlantic, (b) Pacific, (c) North America and (d) Europe regions from the most intensely precipitating 200 ETCs in each region. Figures are in mm day^{-1}. Composites have a 20° radius. The areas enclosed by black contours show where differences between the datasets are statistically significant at ≥95%. In the HiGEM composites, the 95% contour is shown with respect to GPCP. In the ERAI composites, the 95% contour is shown with respect to HiGEM. In the GPCP composites, the 95% contour is shown with respect to ERAI.

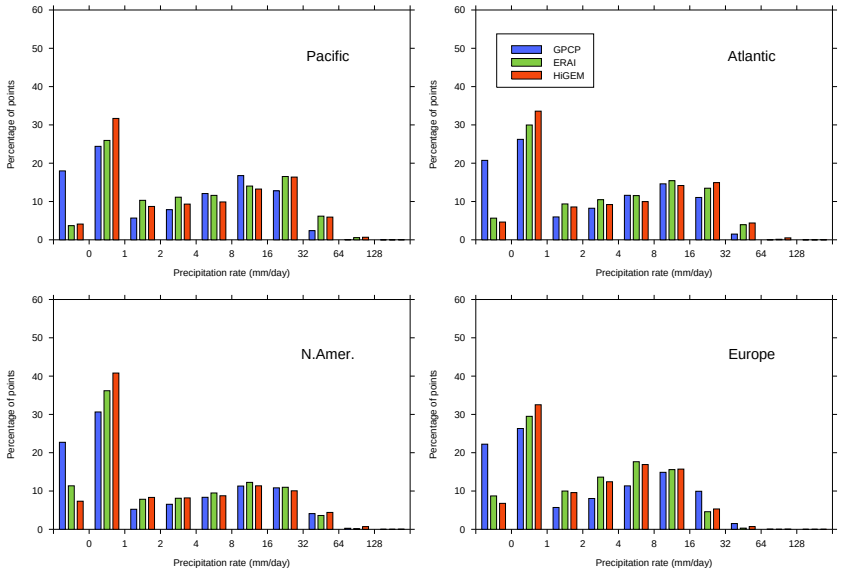

Fig. 4 Distributions of precipitation intensities across all pixels in all 200 storms for a 20° radial cap around the ETC centres for the four regions. The bin at the far left represents 0mm day^{-1} with the remaining bins between the values on the x-axis. Confidence intervals (at 95%) on all histogram bins are less than ±0.21% and are based on the standard error of the mean.

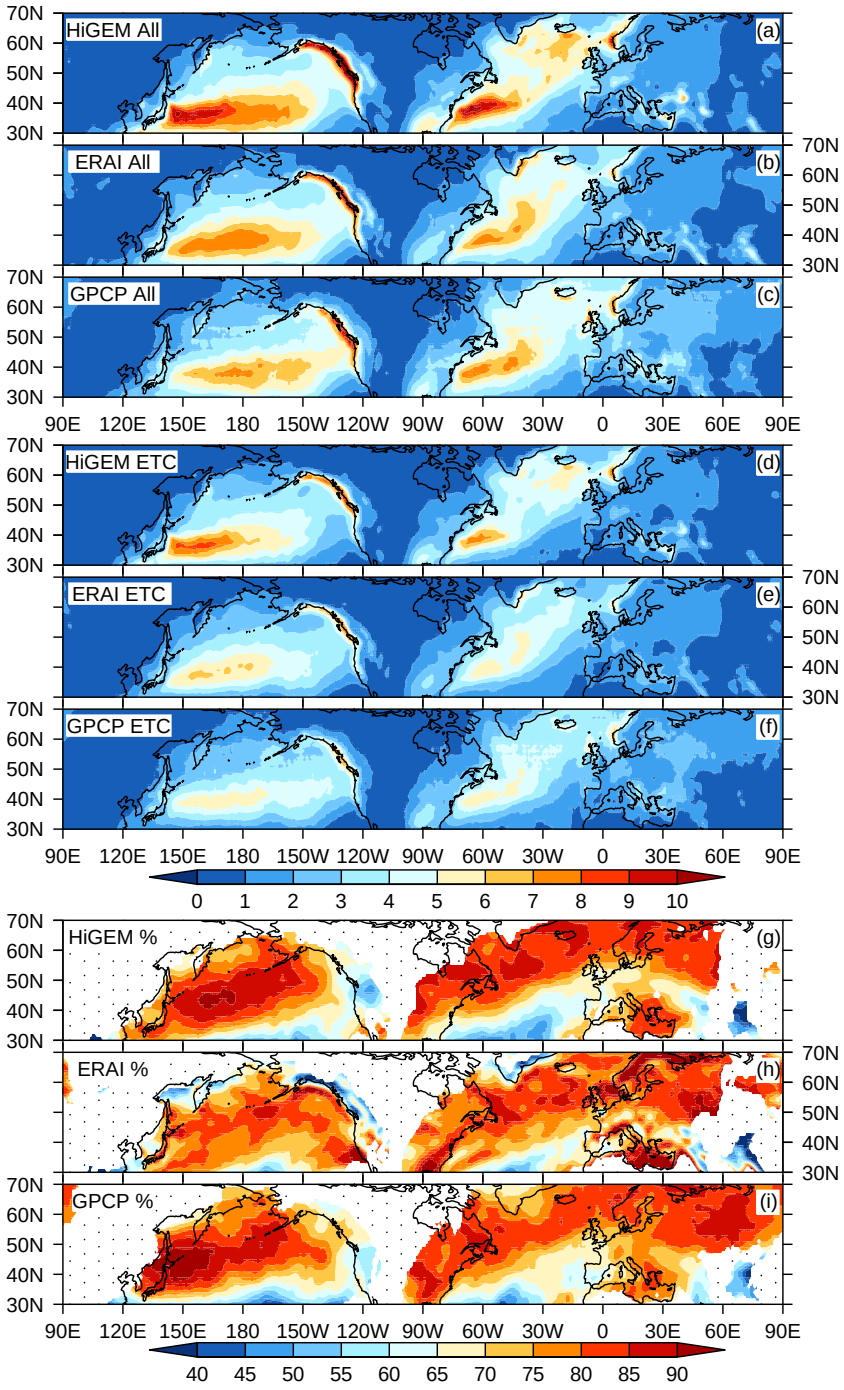

Fig. 5 Total precipitation (All, a-c), storm associated precipitation (ETC, d-f) and the percentage of the total precipitation contributed by ETCs (%, g-i) in HiGEM, ERAI and GPCP. The masked and stippled areas in the percentage plots are where the total climatological precipitation is less than 1mm day^{-1}. Figures are in mm day^{-1} for panels a-f and % for panels g-i.

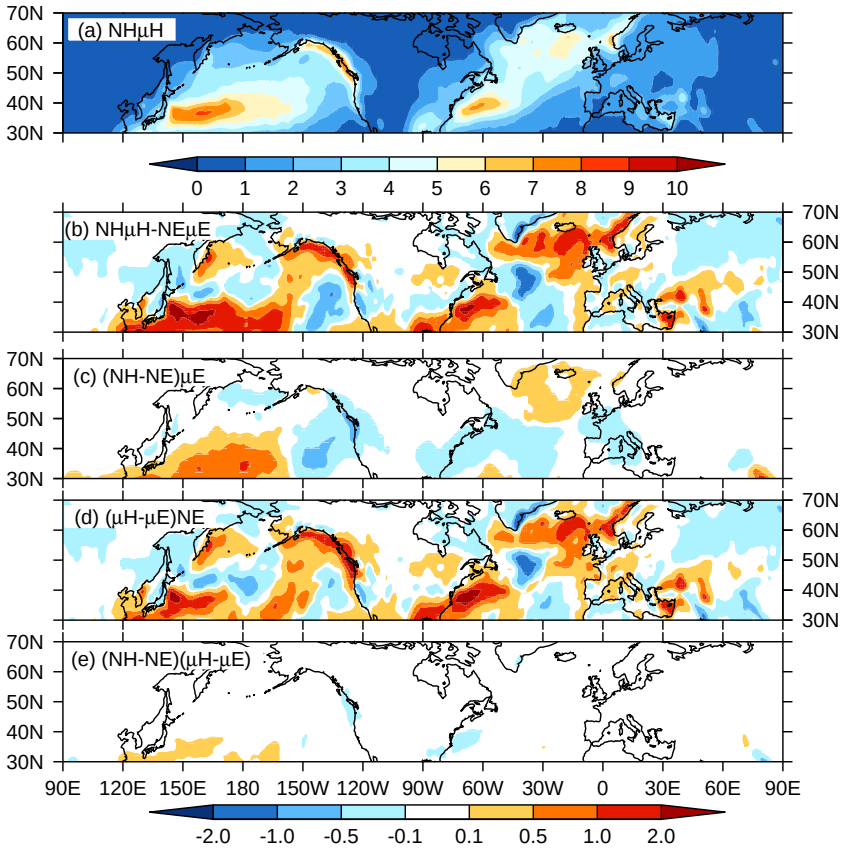

Fig. 6 Storm associated precipitation in (a) HiGEM (NHμH) and the differences in the storm associated precipitation climatology relative to (b) ERAI (NHμH-NEμE) associated with the differences in (c) the number of ETCs ((NH-NE)μE), (d) the average precipitation intensity of ETCs ((μH-μE)NE) and (e) the cross—term ((NH-NE)(μH-μE)). Figures are in mm day^{-1} and are smoothed over 3° to reduce noise. Terms are as in Equation 1.

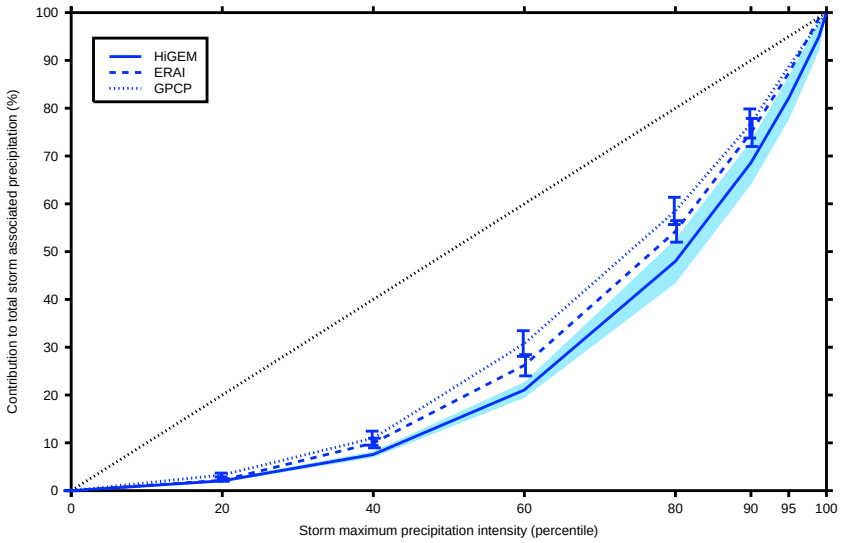

Fig. 7 Contribution to storm associated precipitation based on the maximum precipitation intensity of storms. Maximum intensity is derived from a 5° areal average around the storm centre at the time of peak precipitation. The precipitation associated with storms over their lifetime is then accumulated to derive the importance of storms - based on their maximum intensity - to the total climatological storm associated precipitation. Intensity values are percentiles of all storms in the study period with the contribution shown as a cumulative contribution of all storms below a given percentile threshold. The black dotted line demonstrates the relationship that would exist if all storms contributed equally and demonstrates the importance to the overall climatology of storms of different maximum precipitation intensity. Error bars show the standard deviation of interannual variability for GPCP and ERAI across the decade of data here. The shading shows the standard deviation for HiGEM.

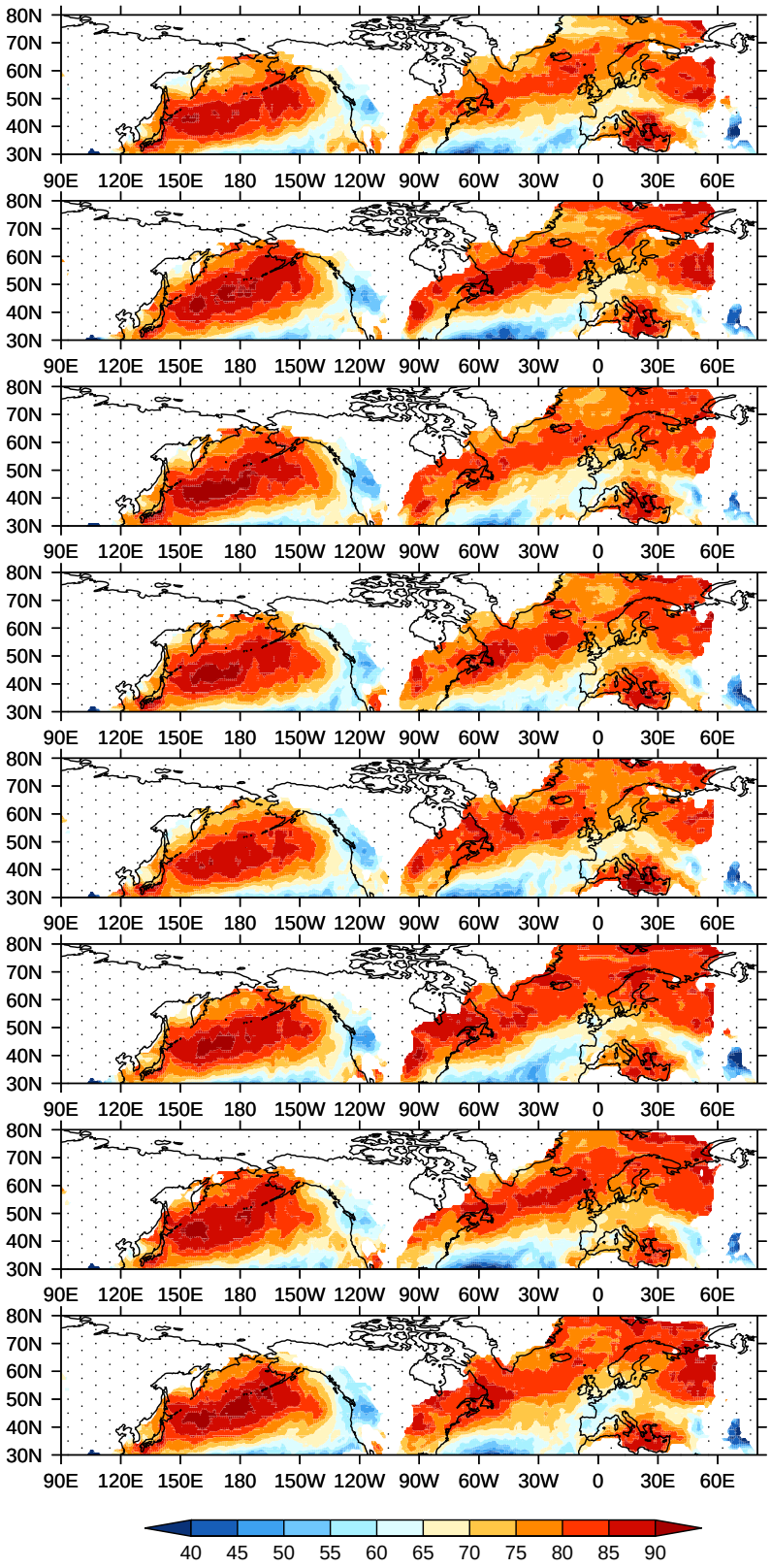

Fig. 8 Decadal variability in the percentage of the total precipitation contributed by ETCs (%) in HiGEM. Each panel represents a single decade from the model integration. The masked and stippled areas in the percentage plots are where the total precipitation for that decade is less than 1mm day^{-1}.

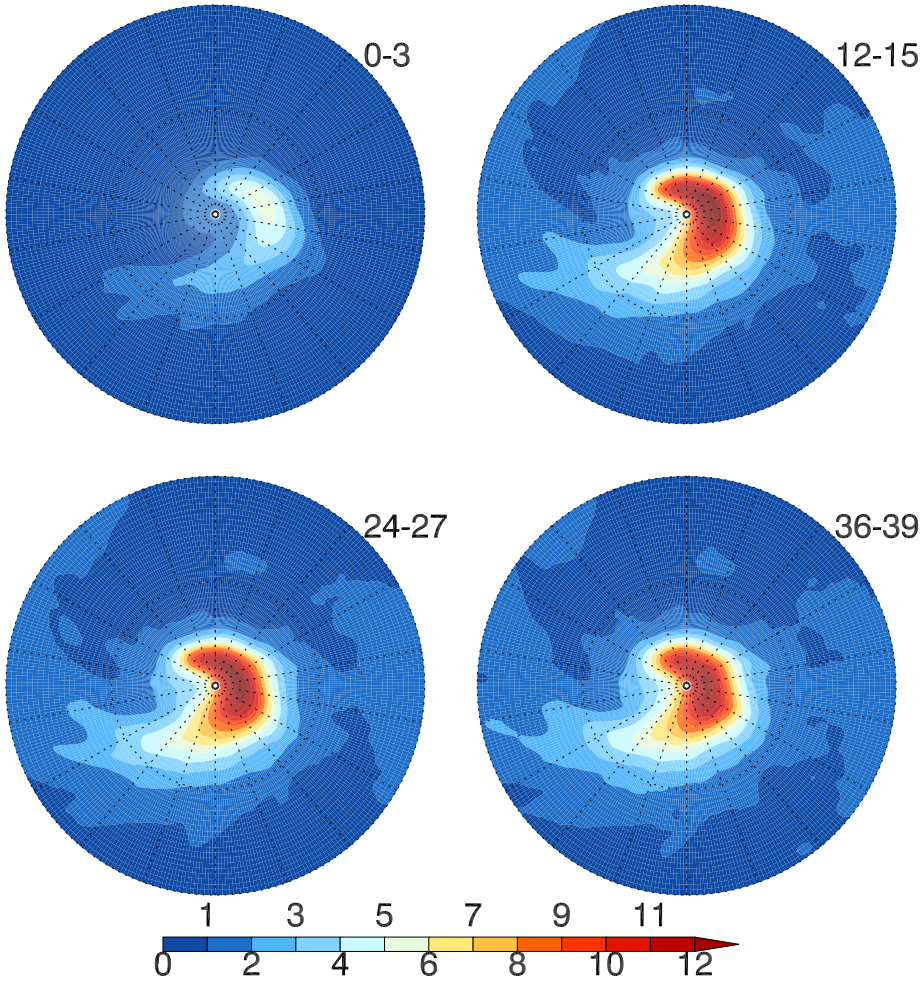

Fig. 9 The effect of spin-up on composite precipitation. The composites are taken from the 200 Atlantic storms shown in Figure 3. Accumulations are shown for leadtimes 0-3, 12-15, 24-27 and 36-39 hours. All figures are expressed in mm day^{-1}. Accumulations are from each 3-hour window.

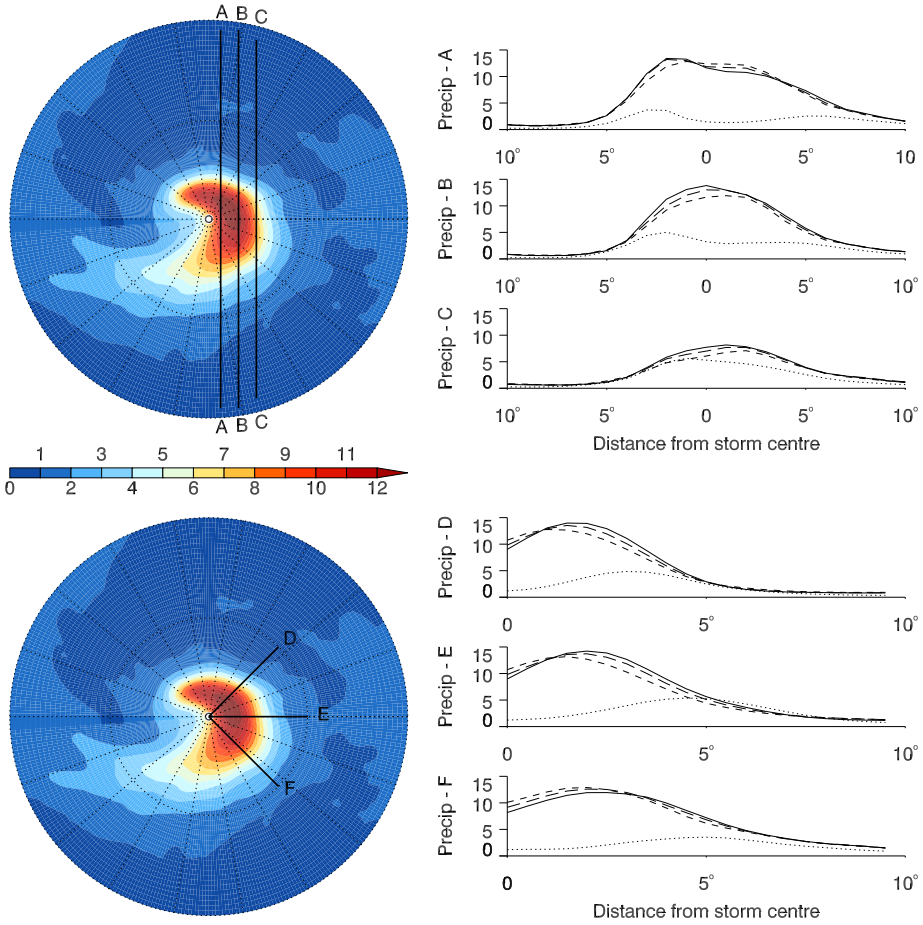

Fig. 10 Composite precipitation intensities. The left panels show a composite at 12-hour lead time, with the locations of the cross-sections (A-F) in the corresponding right hand panels overlaid. Lead times in the right hand panels are 0-3 (dotted line), 12-15 (solid), 24-27 (long dashes) and 36-29 hours (short dashes). All figures in mm day^{-1}. Accumulations are from each 3-hour window.

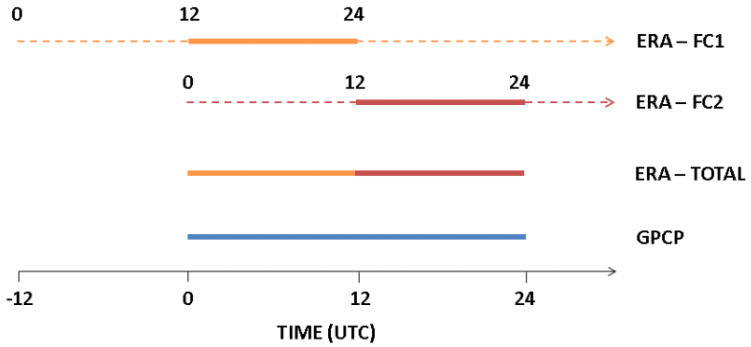

Fig. 11 ERAI precipitation accumulations used for the daily periods in this analysis. Precipitation is extracted from 12-24hours in two forecasts which are initialised at 12UTC on the previous day (FC1) and 00UTC on the day of interest (FC2). The two accumulations are then combined.

References

Adler R, Huffman G, Chang A, Ferraro R, Xie P, Janowiak J, Rudolf B, Schneider U, Curtis S, Bolvin D, et al (2003) The version 2 global precipitation climatology project (GPCP) monthly precipitation analysis (1979-present). Journal of Hydrometeorology 4(6):1147–1167

Bengtsson L, Hodges K, Roeckner E (2006) Storm tracks and climate change. Journal of Climate 19(15):3518–3543

Bengtsson L, Hodges K, Esch M, Keenlyside N, Kornblueh L, Luo J, Yamagata T (2007) How may tropical cyclones change in a warmer climate? Tellus A 59(4):539–561

Bengtsson L, Hodges K, Keenlyside N (2009) Will extratropical storms intensify in a warmer climate? Journal of Climate 22(9):2276–2301

Bolvin DT, Adler RF, Huffman GJ, Nelkin EJ, Poutiainen JP (2009) Comparison of GPCP Monthly and Daily Precipitation Estimates with High-Latitude Gauge Observations. Journal of Applied Meteorology & Climatology 48(9)

Butler AH, Thompson DW, Heikes R (2010) The Steady-State Atmospheric Circulation Response to Climate Change–like Thermal Forcings in a Simple General Circulation Model. Journal of Climate 23(13)

Catto J, Pfahl S (2013) The importance of fronts for extreme precipitation. Journal of Geophysical Research: Atmospheres 118(19):10–791

Catto J, Shaffrey L, Hodges K (2010) Can Climate Models Capture the Structure of Extratropical Cyclones? J Climate 23:1621–1635

Catto J, Jakob C, Berry G, Nicholls N (2012) Relating global precipitation to atmospheric fronts. Geophysical Research Letters 39(10):L10,805

Catto J, Jakob C, Nicholls N (2013) A global evaluation of fronts and precipitation in the ACCESS model. Aust Meteorol Ocean Soc J 63:191–203

Catto JL, Shaffrey LC, Hodges KI (2011) Northern hemisphere extratropical cyclones in a warming climate in the HiGEM high-resolution climate model. Journal of Climate 24(20):5336–5352

Crétat J, Vizy EK, Cook KH (2014) How well are daily intense rainfall events captured by current climate models over Africa? Climate Dynamics 42(9-10):2691–2711

622 Dacre H, Hawcroft M, Stringer M, Hodges K (2012) IN BOX-An Extratropical Cyclone Atlas-
623 A Tool for Illustrating Cyclone Structure and Evolution Characteristics. Bulletin of the
624 American Meteorological Society 93(10):1497
625 Dacre H, Clark P, Martinez-Alvarado O, Stringer M, Lavers D (2014) How do atmospheric
626 rivers form? Bulletin of the American Meteorological Society
627 Dacre HF, Gray SL (2013) Quantifying the climatological relationship between extratropical
628 cyclone intensity and atmospheric precursors. Geophysical Research Letters 40(10):2322–
629 2327
630 Davies T, Cullen MJP, Malcolm AJ, Mawson MH, Staniforth A, White AA, Wood N (2005) A
631 new dynamical core for the Met Office's global and regional modelling of the atmosphere.
632 Quarterly Journal of the Royal Meteorological Society 131:1759–1782
633 Dee D, Uppala S, Simmons A, Berrisford P, Poli P, Kobayashi S, Andrae U, Balmaseda M,
634 Balsamo G, Bauer P, et al (2011) The ERA-Interim reanalysis: Configuration and per-
635 formance of the data assimilation system. Quarterly Journal of the Royal Meteorological
636 Society 137(656):553–597
637 Della-Marta P, Luterbacher J, Von Weissenfluh H, Xoplaki E, Brunet M, Wanner H (2007)
638 Summer heat waves over western Europe 1880–2003, their relationship to large-scale forc-
639 ings and predictability. Climate Dynamics 29(2-3):251–275
640 Ferranti L, Viterbo P (2006) The European summer of 2003: Sensitivity to soil water initial
641 conditions. Journal of Climate 19(15):3659–3680
642 Field P, Wood R (2007) Precipitation and cloud structure in midlatitude cyclones. Journal of
643 climate 20(2):233–254
644 Finnis J, Holland M, Serreze M, Cassano J (2007) Response of Northern Hemisphere extrat-
645 ropical cyclone activity and associated precipitation to climate change, as represented by
646 the Community Climate System Model. J Geophys Res 112:G04S42
647 Froude LS, Bengtsson L, Hodges KI (2007a) The predictability of extratropical storm tracks
648 and the sensitivity of their prediction to the observing system. Monthly weather review
649 135(2)
650 Froude LS, Bengtsson L, Hodges KI (2007b) The prediction of extratropical storm tracks by
651 the ECMWF and NCEP ensemble prediction systems. Monthly weather review 135(7)

652 Harvey B, Shaffrey L, Woollings T (2014) Equator-to-pole temperature differences and the
653 extra-tropical storm track responses of the CMIP5 climate models. Climate Dynamics
654 43(5-6):1171–1182
655 Hawcroft M, Shaffrey L, Hodges K, Dacre H (2012) How much Northern Hemisphere precipi-
656 tation is associated with extratropical cyclones? Geophysical Research Letters 39(24)
657 Held I (1993) Large-scale dynamics and global warming. Bulletin of the American Meteoro-
658 logical Society 74(2):228–242
659 Hodges K (1994) A General Method for Tracking Analysis and Its Application to Meteorolog-
660 ical Data. Mon Wea Rev 122:2573–2586
661 Hodges K (1995) Feature tracking on the unit sphere. Mon Wea Rev 123:3458–3465
662 Hodges K (1999) Adaptive Constraints for Feature Tracking. Mon Wea Rev 127:1362–1373
663 Hodges K, Lee R, Bengtsson L (2011) A Comparison of Extratropical Cyclones in Recent
664 Reanalyses ERA-Interim, NASA MERRA, NCEP CFSR, and JRA-25. Journal of Climate
665 24(18)
666 Hoskins B, Hodges K (2002) New perspectives on the Northern Hemisphere winter storm
667 tracks. Journal of the Atmospheric Sciences 59(6):1041–1061
668 Hou A, Zhang S, da Silva A, Olson W, Kummerow C, Simpson J (2001) Improving global
669 analysis and short-range forecast using rainfall and moisture observations derived from
670 TRMM and SSM/I passive microwave sensors. Bulletin of the American Meteorological
671 Society 82(4):659–680
672 Huffman G, Adler R, Morrissey M, Bolvin D, Curtis S, Joyce R, McGavock B, Susskind J (2001)
673 Global Precipitation at One-Degree Daily Resolution from Multi-Satellite Observations. J
674 Hydrometeor 2:36–50
675 Huffman GJ, Adler RF, Bolvin DT, Gu G (2009) Improving the global precipitation record:
676 GPCP version 2.1. Geophysical Research Letters 36(17)
677 John VO, Allan RP, Soden BJ (2009) How robust are observed and simulated precipitation
678 responses to tropical ocean warming? Geophysical Research Letters 36(14)
679 Johns TC, Durman CF, Banks HT, Roberts MJ, McLaren AJ, Ridley JK, Senior CA, Williams
680 KD, Jones A, Rickard GH, Cusack S, Ingram WJ, Crucifix M, Sexton DMH, Joshi MM,
681 Dong BW, Spencer H, Hill RSR, Gregory JM, Keen AB, Pardaens AK, Lowe JA, Bodas-

682 Salcedo A, Stark S, Searl Y (2006) The new Hadley Centre Climate Model (HadGEM1):
683 Evaluation of Coupled Simulations. Journal of Climate 19:1327–1353
684 Joos H, Wernli H (2011) Influence of microphysical processes on the potential vorticity de-
685 velopment in a warm conveyor belt: a case-study with the limited-area model COSMO.
686 Quarterly Journal of the Royal Meteorological Society 138(663):407–418
687 Joshi MK, Rai A, Pandey A (2013) Validation of TMPA and GPCP 1DD against the ground
688 truth rain-gauge data for Indian region. International Journal of Climatology 33(12):2633–
689 2648
690 Kållberg P (2011) Forecast drift in ERA-Interim. European Centre for Medium Range Weather
691 Forecasts
692 Kaspi Y, Schneider T (2013) The Role of Stationary Eddies in Shaping Midlatitude Storm
693 Tracks. Journal of the Atmospheric Sciences 70(8)
694 Keeley S, Sutton R, Shaffrey L (2012) The impact of North Atlantic sea surface temperature
695 errors on the simulation of North Atlantic European region climate. Quarterly Journal of
696 the Royal Meteorological Society 138(668):1774–1783
697 Kendon EJ, Roberts NM, Senior CA, Roberts MJ (2012) Realism of rainfall in a very high-
698 resolution regional climate model. Journal of Climate 25(17):5791–5806
699 Kobold M, Sušelj K (2005) Precipitation forecasts and their uncertainty as input into hydro-
700 logical models. Hydrology & Earth System Sciences 9(4)
701 Kummerow C, Berg W, Thomas-Stahle J, Masunaga H (2006) Quantifying global uncertainties
702 in a simple microwave rainfall algorithm. Journal of Atmospheric and Oceanic Technology
703 23(1):23–37
704 de Leeuw J, Methven J, Blackburn M (2014) Evaluation of ERA-Interim reanalysis precip-
705 itation products using England and Wales observations. Quarterly Journal of the Royal
706 Meteorological Society
707 Lim EP, Simmonds I (2009) Effect of tropospheric temperature change on the zonal mean
708 circulation and SH winter extratropical cyclones. Climate dynamics 33(1):19–32
709 Martin GM, Ringer MA, Pope VD, Lones A, Dearden C, Hinton TJ (2006) The Physical
710 Properties of the Atmosphere in the New Hadley Centre Global Environmental Model
711 (HadGEM1). Part I: Model Description and Global Climatology. Journal of Climate

712 19:1274–1301

713 McLaren A, Banks H, Durman C, Gregory J, Johns T, Keen A, Ridley J, Roberts M, Lipscomb
714 W, Connolley W, et al (2006) Evaluation of the sea ice simulation in a new coupled
715 atmosphere-ocean climate model (HadGEM1). Journal of Geophysical Research: Oceans
716 (1978–2012) 111(C12)

717 McPhee J, Margulis SA (2005) Validation and error characterization of the GPCP-1DD pre-
718 cipitation product over the contiguous united states. Journal of Hydrometeorology 6(4)

719 Nicholson SE, Some B, McCollum J, Nelkin E, Klotter D, Berte Y, Diallo B, Gaye I, Kpabeba
720 G, Ndiaye O, et al (2003) Validation of TRMM and other rainfall estimates with a high-
721 density gauge dataset for West Africa. Part I: Validation of GPCC rainfall product and
722 pre-TRMM satellite and blended products. Journal of Applied Meteorology 42(10)

723 Pearson K, Shaffrey L, Methven J, Hodges K (2014) Can a climate model reproduce extreme
724 regional precipitation events over England and Wales? Quarterly Journal of the Royal
725 Meteorological Society

726 Peixoto JP, Oort AH (1992) Physics of climate. American Institute of Physics, New York

727 Pfahl S, Wernli H (2012) Quantifying the relevance of cyclones for precipitation extremes. J
728 Climate

729 Pitt M (2008) The Pitt Review - Learning Lessons from the 2007 floods. Final report available
730 at http://archive.cabinetoffice.gov.uk/pittreview/thepittreview/final_report.html

731 Rossow WB, Mekonnen A, Pearl C, Goncalves W (2013) Tropical precipitation extremes.
732 Journal of Climate 26(4):1457–1466

733 Roy P, Gachon P, Laprise R (2014) Sensitivity of seasonal precipitation extremes to model
734 configuration of the Canadian Regional Climate Model over eastern Canada using historical
735 simulations. Climate Dynamics pp 1–23

736 Rudeva I, Gulev SK (2011) Composite Analysis of North Atlantic Extratropical Cyclones in
737 NCEP–NCAR Reanalysis Data. Monthly Weather Review 139(5)

738 Shaffrey L, Stevens I, Norton W, Roberts M, Vidale P, Harle J, Jrrar A, Stevens D, Woodage
739 M, Demory M, et al (2009) UK HiGEM: the new UK high-resolution global environment
740 model-model description and basic evaluation. Journal of Climate 22(8):1861–1896

741 Sibley A (2010) Analysis of extreme rainfall and flooding in Cumbria 18–20 November 2009.
742 Weather 65(11):287–292
743 Simmons A, Uppala S, Dee D, Kobayashi S (2007) ERA-Interim: New ECMWF reanalysis
744 products from 1989 onwards. ECMWF newsletter 110:25–35
745 Simmons A, Willett K, Jones P, Thorne P, Dee D (2010) Low-frequency variations in
746 surface atmospheric humidity, temperature, and precipitation: Inferences from reanal-
747 yses and monthly gridded observational data sets. Journal of Geophysical Research
748 115(D1):D01,110
749 Stephens G, L'Ecuyer T, Forbes R, Gettlemen A, Golaz J, Bodas-Salcedo A, Suzuki K, Gabriel
750 P, Haynes J (2010) Dreary state of precipitation in global models. Journal of Geophysical
751 Research 115(D24):D24,211
752 Trenberth K (1999) Conceptual framework for changes of extremes of the hydrological cycle
753 with climate change. Climatic Change 42(1):327–339
754 Ulbrich U, Brücher T, Fink A, Leckebusch G, Krüger A, Pinto J (2003) The central European
755 floods of August 2002: Part 1–Rainfall periods and flood development. Weather 58(10):371–
756 377
757 Uppala SM, Kallberg PW, Simmons AJ, Andrae U, Da Costa Bechtold V, Fiorino M, Gibson
758 JK, Haseler J, Hernandez A, Kelly GA, Li X, Onogi K, Saarinen S, Sokka N, Allan RP,
759 Andersson E, Arpe K, Balmaseda MA, Beljaars ACM, Van De Berg L, Bidlot J, Bormann
760 N, Caires S, Chevallier F, Dethof A, Dragosavac M, Fisher M, Fuentes M, Hagemann
761 S, Holm E, Hoskins BJ, Isaksen L, Janssen PAEM, Jenne R, McNally AP, Mahfouf JF,
762 Morcrette JJ, Rayner NA, Saunders RW, Simon P, Sterl A, Trenberth KE, Untch A,
763 Vasiljevic D, Viterbo P, Woollen J (2005) The ERA-40 re-analysis. Quarterly Journal of
764 the Royal Meteorological Society 131(612):2961–3012
765 Vautard R, Yiou P, D'Andrea F, De Noblet N, Viovy N, Cassou C, Polcher J, Ciais P,
766 Kageyama M, Fan Y (2007) Summertime European heat and drought waves induced by
767 wintertime Mediterranean rainfall deficit. Geophysical Research Letters 34(7)
768 Wang G, Dolman A, Alessandri A (2011) A summer climate regime over Europe modulated
769 by the North Atlantic Oscillation. Hydrology and Earth System Sciences 15(1):57–64

Willison J, Robinson WA, Lackmann GM (2013) The Importance of Resolving Mesoscale Latent Heating in the North Atlantic Storm Track. Journal of the Atmospheric Sciences 70(7)

Woollings T (2010) Dynamical influences on European climate: an uncertain future. Philosophical Transactions of the Royal Society A: Mathematical, Physical and Engineering Sciences 368(1924):3733–3756

Zappa G, Shaffrey L, Hodges K (2013) The ability of CMIP5 models to simulate North Atlantic extratropical cyclones. Journal of Climate 26(15)

Zappa G, Hawcroft MK, Shaffrey L, Black E, Brayshaw DJ (2014) Extratropical cyclones and the projected decline of winter Mediterranean precipitation in the CMIP5 models. Climate Dynamics pp 1–12